frontiers | Frontiers in Earth Science

ORIGINAL RESEARCH
published: 01 June 2022
doi: 10.3389/feart.2022.916044

Deep Electrical Structure of the Langshan Mountain-Linhe Basin Area on the Northwest Edge of the Ordos Block, China

Lingqiang Zhao[1,2]*, *Qingliang Wang*[2], *Cong Cao*[2] and *Ming Hao*[2]

[1]State Key Laboratory of Earthquake Dynamics, Institute of Geology, China Earthquake Administration, Beijing, China, [2]The Second Monitoring and Application Center, China Earthquake Administration, Xi'an, China

A series of fault depression structures have developed around the Ordos Block. The Langshan Mountain-Linhe Basin area (LLA), located on the northwest edge of the Ordos Block, is a typical, normal tension fault system. A geological survey shows that the Langshan Piedmont fault (LPF) in this area has a large slip rate and indicates risk of earthquake preparation. Broadband magnetotelluric (MT) exploration research was recently carried out across the LLA in the NW–SE direction, and the three-dimensional deep electrical structure thus obtained revealed that the LPF in the LLA is an evident electrical boundary zone on the whole crustal scale and is the main boundary fault of the primary structural block of the Alxa and Ordos Blocks. The MT results also show that the Linhe Basin and Ordos Block belong to the same tectonic basement. The Linhe and Dengkou faults belong to the internal faults of the Ordos Block. The upper crust of the Langshan Mountain on the west side of LPF is characterized by high-resistivity, the middle and lower crust have a low-resistivity layer, and the Linhe Basin on the east side has a Cenozoic low-resistivity sedimentary layer of approximately 10 km thick, which reveals that the Linhe Basin is a faulted basin with sedimentary thickness around the Ordos Block. This indicates that the LLA has experienced continuous and strong tension, normal fault depression sedimentary activities since the Cenozoic era. The current Global Positioning System velocity field shows that there is an apparent NW–SE acceleration zone in the LLA. The leveling data indicate that Linhe Basin shows a subsidence trend relative to the Ordos Block, indicating that the area is undergoing continuous NW–SE tension and faulting. It is speculated that there is a risk of earthquake preparation in the LPF.

Keywords: magnetotelluric, electrical structure, Langshan Piedmont fault, Linhe Basin, low-resistivity sedimentary layer

OPEN ACCESS

Edited by:
Wenjun Zheng,
Sun Yat-sen University, Zhuhai Campus, China

Reviewed by:
Zhen Guo,
Southern University of Science and Technology, China
Xuzhang Shen,
Sun Yat-sen University, China
Shaopeng Dong,
China Earthquake Administration, China

****Correspondence:***
Lingqiang Zhao
zhaolingqiang0926@126.com

Specialty section:
This article was submitted to Geohazards and Georisks, a section of the journal Frontiers in Earth Science

Received: *08 April 2022*
Accepted: *16 May 2022*
Published: *01 June 2022*

Citation:
Zhao L, Wang Q, Cao C and Hao M (2022) Deep Electrical Structure of the Langshan Mountain-Linhe Basin Area on the Northwest Edge of the Ordos Block, China. Front. Earth Sci. 10:916044. doi: 10.3389/feart.2022.916044

1 INTRODUCTION

There are a series of extensional basin-mountain faulted structural areas around the Ordos Block, such as the Langshan Mountain-Linhe Basin area (LLA) on the northwest edge of the Ordos Block (**Figure 1B**), Helanshan Mountain-Yinchuan Basin faulted structural area on the west edge, Qinling Mountain-Weihe Basin faulted structural area on the south edge, and Lvliangshan Mountain-Linfen

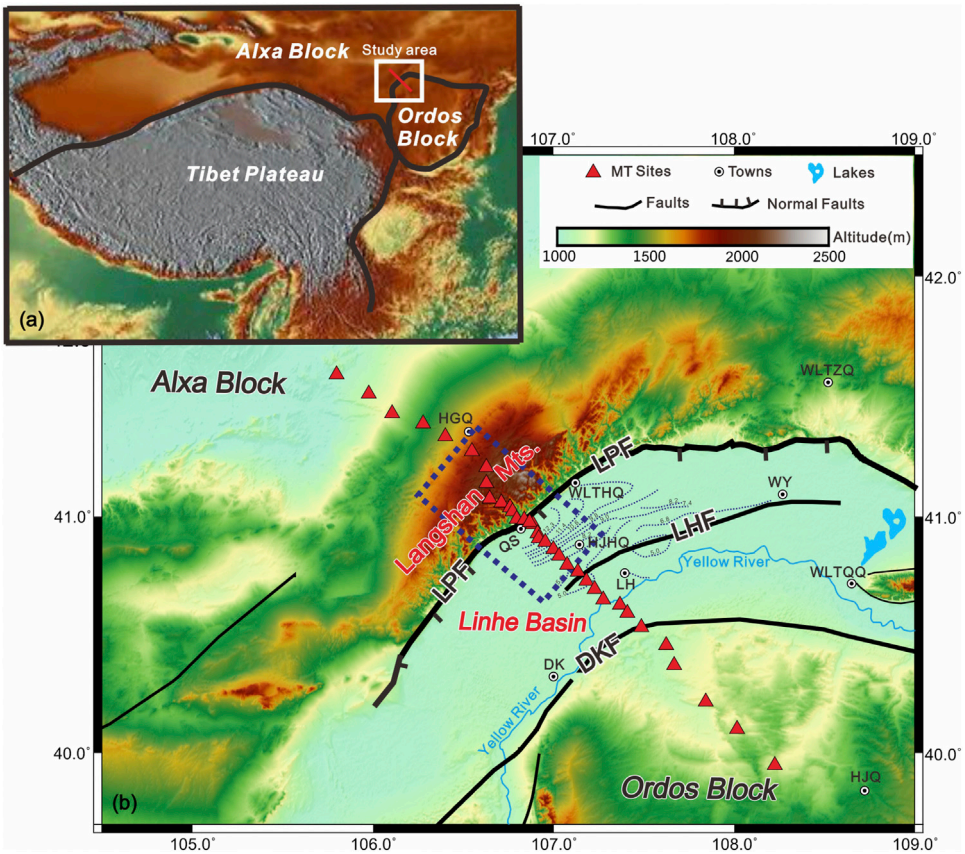

FIGURE 1 | Regional tectonic setting **(A)** distribution map of faults and magnetotelluric (MT) sites on the northwest edge of Ordos Block **(B)** The thickness of the Cenozoic sedimentary layer is quoted from the State Seismological Bureau (1988). LPF, Langshan Piedmont fault; LHF, Linhe fault; DKF, Dengkou fault; QS, Qingshan; HJHQ, Hangjinhouqi; LH, Linhe; DK, Dengkou; WH, Wuhai; WLTHQ, Wulatehouqi; WY, Wuyuan; WLTQQ, Wulateqianqi; WLTZQ, Wulatezhongqi; HJQ, Hangjinqi.

Basin on the east edge. These basin-fault rift tectonic areas are often strong earthquake preparedness zones for the Chinese mainland (State Seismological Bureau, 1988). In 1739, the Pingluo M8 earthquake occurred in the faulted structural area of Helanshan Mountain-Yinchuan Basin, causing more than 50,000 casualties (Lei et al., 2015). The Huashan earthquake occurred in the faulted structural area of the Qinling Mountain-Weihe Basin in 1,556 and was the most serious natural disaster in Chinese historical records (Hou et al., 1998; Rao et al., 2014; Du et al., 2017; Feng et al., 2020). The Hongdong M8 earthquake occurred in the structural area of the Lvliangshan Mountain-Linfen Basin in 1,303 (Deng et al., 2003; Xu et al., 2018). These areas have been the key research areas in the field of Geosciences in recent years. The LLA is located in the northern part of the north-south seismic belt of the Chinese mainland, and it is also subjected to the northeast (NE) pushing of the Tibetan Plateau and northwest-southeast (NW–SE) tensioning caused by deep subduction of the Pacific plate (Northrup et al., 1995; Zhang et al., 2006). The Langshan Piedmont fault (LPF) in this structural area is a large fault that controls the NW boundary of the Hetao Basin (the Linhe Basin belongs to the western region of the Hetao Basin. The Hetao Basin can be divided into three secondary depressions from west to east: Linhe Basin, Baiyanhua Basin, and Huhe Basin), and may also be the boundary fault between the Alxa and Ordos Blocks (State Seismological Bureau, 1988; Rao et al., 2016; Zhang et al., 2020). Geological surveys show that activity of the LPF, especially in the middle section, is very intense (Dong et al., 2016; Rao et al., 2016; Dong et al., 2018a; 2018b). Dong et al. (2018a) and Rao et al. (2016) revealed that the fault is an important seismic zone in the Hetao Basin through trenching, dating, and other methods. The average recurrence period of strong earthquakes is about 2,500 A, and the average magnitude of each earthquake reaches 7–8 (Dong et al., 2018a, 2018b; Liang et al., 2021). At present, the recurrence period of strong earthquakes at the fault has been exceeded, so there is a great possibility of destructive, strong earthquakes occurring again (Dong et al., 2018a). Li et al. (2015) and Rao et al. (2016) believe that the latest earthquake rupture event of LPF may be related to the great earthquake in 7 BC. Liang et al. (2021) believe that the magnitude of the earthquake in 7 BC reached 8.1, and there is still a risk of magnitude 7.4–8.0 earthquakes in this area. Due to the lack of large earthquakes recorded by modern instruments in the fault depression structural area of LLA, the existing research results in this area focus on geomorphology and paleoseismology (Jia et al., 2016; Rao et al., 2016; He et al., 2017, 2018; Dong et al., 2018a, 2018b, 2018c; He et al., 2020; Zhang

et al., 2020; Li J. et al., 2021; Liang et al., 2021; Xu et al., 2022). The results obtained lack the support of deep geophysical data. The Linhe Basin has had a relatively developed economy and society since ancient times; there are important towns such as Linhe (LH), Hangjinhouqi (HJHQ), and Wulatehouqi (WLTHQ) with large population densities. Therefore, the deep distribution of faults and seismic risk in the structural area of LLA is of great concern.

Wu et al. (2022) recently obtained the large-scale, three-dimensional (3D) S-wave velocity structure of the crust and upper mantle of the Ordos Block and its surrounding areas and found that there is a thickening of the Cenozoic sedimentary layer in the Linhe Basin. Chen et al. (2020) revealed that the Moho depth of Alxa Block is 38–45 km, that of Ordos Block is 38–42 km, and that of LLA in the transition zone is 52 km. Seismology also shows that there are obvious differences in the crustal structure between the Alxa and Ordos Blocks (Chen et al., 2020). It is speculated that the Alxa and Ordos Blocks belong to different tectonic units. Chang et al. (2011) found that the anisotropic fast wave direction in LLA was in a NW–SE direction when summarizing the anisotropic characteristics of the Ordos Block and surrounding upper mantle, which indicates that there may be NW–SE stretching in this area. Numerical simulation shows that the lateral horizontal movement of the stable Ordos Block has good integrity (Chen et al., 2011). Scholars have carried out Coulomb stress statistics (Zhang et al., 2021), anisotropy analysis (Hu et al., 2011), and crustal strain analysis (Cui et al., 2016) in the LLA on the northwest edge of the Ordos Block and have concluded that the LLA is in a state of tensile strain. The results of multi-scale tomography reveal that the northwest edge of the Ordos Block may have experienced mantle thermal material upwelling, transforming the lithospheric structure (Gao et al., 2018). These research results focus on crustal deformation and large-scale geophysical imaging; there is a lack of research on the fine structure of deep faults, especially fine, deep, geophysical exploration near the LPF.

The electrical structural information of the crust obtained using the magnetotelluric (MT) method can provide a basis for the division of block units (Chen., 1990). It is an important deep geophysical method used to detect the deep extension characteristics of the fault zone and has been widely used (Zhao et al., 2012; Cai et al., 2017; Yu et al., 2017; Wang et al., 2018; Hu et al., 2020; Sun et al., 2020; Li L. et al., 2021; Ye et al., 2021; Zhan et al., 2021; Zhao et al., 2021; Chang et al., 2022; Zhao et al., 2022). Predecessors have completed much MT exploration work in the Ordos Block and its surrounding areas. The Ordos Block belongs to a stable block unit and is in contact with the surrounding blocks (Zhao et al., 2004, 2010; Dong et al., 2014; Li et al., 2017; Xu et al., 2017; Zhan et al., 2017; Han et al., 2022). The LLA in the contact area between the Ordos and Alxa Blocks lacks MT exploration results. Therefore, we completed a broadband MT profile with a length of more than 270 km passing through the LLA. The MT profile started from the Alxa Block in the west and extended to the Ordos Block in the east. The data were inversed and used to calculate the deep electrical structural information of the area. From the perspective of electrical structure, this paper discusses the deep structural characteristics of LLA and its adjacent areas, and further evaluates the contact relationship between the Ordos and Alxa Blocks, and then discusses the dynamic background of LLA and the earthquake breeding risk of LPF in combination with the regional 3D deformation field data. The results obtained can advocate the seismic risk assessment of LLA, and can also provide deep geophysical data for the formation mechanism of faulted basins around the Ordos Block.

2 GEOLOGIC SETTING

LLA is located in the contact area between the Alxa and Ordos Blocks, which is a part of Hetao Graben (Rao et al., 2016; Zhang et al., 2020), The LPF is located at the southeast foot of the NE-trending Langshan Mountain. It intersects with the EW-trending Sertengshan Piedmont fault in the north and terminates in Ulanbuhe Desert in the southwest. The total length of the LPF is approximately 160 km and the overall strike is NE 55°. The overall tendency of the fault is SW (Dong et al., 2018a; 2018b). According to the block division theory of Deng et al. (2003), LPF is the boundary fault between the Ordos and Alxa Blocks. The Langshan Mountain on the west side of the fault belongs to the Alxa Block, and the Linhe Basin on the east side of the fault belongs to the Ordos Block (Rao et al., 2016; Zhang et al., 2020). Previous researchers have summarized (State Seismological Bureau, 1988; Dong et al., 2016; Dong et al., 2018a, 2018b; He et al., 2020; Liang et al., 2021) the evolutionary history of multiple stages in the LLA: 1) Oligocene stage: This was the initial developmental stage of LLA. Due to the activity of LPF and the relative uplifting of the mountain, the Linhe Basin began to form. The sedimentary thickness of the subsidence center was 2,400 m and the subsidence rate was 0.10 mm/a (State Seismological Bureau, 1988). The maximum thickness of the stratum was mainly distributed along the LPF. 2) Late tertiary stage: This was the most active stage in the development of the LLA. The Linhe Basin continued to decline strongly under the control of the Piedmont faults, with a sedimentary thickness of 3,800 m and a subsidence rate of 0.20 mm/a. 3) In the Pliocene stage, the faulting was more intense, the sedimentary range was further expanded, the thickness reached 6,000 m, and the settlement rate was 0.64 mm/a. 4) In the Quaternary period, the Piedmont Fault activity was still relatively strong, generally faulting the Quaternary system, and the fault activity has maintained its characteristics since the late Tertiary. The mountain rose slowly and the basin continued to settle. The thickness of the Quaternary system was 2,400 m and the settlement rate was 1.00 mm/a. Drilling and petroleum geological profile data (State Seismological Bureau, 1988; Liang et al., 2021) show that Linhe Basin is a sedimentary basin with the largest sedimentary layer thickness around the Ordos Block and is much higher than that of other basins around the Ordos Block over the same period, possibly exceeding 10 km near HJHQ. This shows that the Linhe Basin has a high subsidence rate, which should correspond to very strong fault depression sedimentary activities.

3 MT METHOD AND DATA PROCESSING

3.1 Introduction to the MT Method

The core of the MT method is to determine the underground conductivity structure by using the Earth's external magnetic field and electric field, which vary with time. Specifically, conductivity or resistivity can be determined by the dependence of amplitude and the phase relationship between the electrical field and the magnetic field vector on the Earth's surface. These relationships are expressed in the frequency domain by the correlation transfer function between the surface components of the electromagnetic field, which normalizes the induced response of the magnetic field fluctuation intensity. The transfer function is represented by the impedance tensor, Z, which is defined as:

$$E = ZH, \quad (1)$$

where E is the electric field vector and H is the magnetic field vector (Chen et al., 1990).

In recent years, with the application of supercomputers and the increasingly mature and practical MT 3D inversion algorithms (Siripunvaraporn et al., 2005; Egbert et al., 2012; Kelbert et al., 2014), 3D inversion technology has been widely used in the practical research of various MT detections (Dong et al., 2014; Sun et al., 2019, 2020; Zhao et al., 2022).

3.2 MT Profile and Data Acquisition

The field data acquisition of LLA was carried out from September to October 2021 and took approximately 35 days. Four sets of MTU-5A equipment (Phoenix Company, Canada) were used for data acquisition at the same time (frequency band range 320–0.0005 Hz). The completed MT profile started from Alxa Block in the border area between China and Mongolia in the northwest, passed through LLA in the southeast, exited the Langshan Mountain near Qingshan (QS), entered Linhe Basin, passed through the Yellow River, entered the hinterland of the Ordos Block, and finally terminated near HJQ (**Figure 1B**). The contact area between the Langshan Mountain and the Linhe Basin is the area through which LPF passes, and it is also the key area of this study (as shown by the blue empty frame in **Figure 1B**). A total of 34 MT sites were obtained along the profile. The profile was ~270 km long and densified to 2–3 km near the LPF, which was mainly used to obtain the fine electrical structural information of the LPF area. Due to the relatively simple structure in the peripheral Alxa and Ordos Blocks, the MT site spacing was increased to 10–20 km, which was mainly used to obtain the large-scale, regional electrical structural information (**Figure 1B**).

3.3 Electrical Orientation Analysis

The phase tensor decomposition technique can be used to obtain the electrical orientation information of the MT profile (Caldwell et al., 2004). The rose-petal diagram of the electrical orientation of the full frequency band and sub-band of all 34 MT sites along the profile was calculated using the phase tensor decomposition method in the MTP software developed by Chen et al. (2004). The rose petal diagram of electrical orientation indicates that the electrical orientation of the full frequency band of all sites along the profile is NE 60° or NW 30° (**Figure 2A**). Combined with the tectonic characteristics of the Langshan mountain, LPF, LHF, and DKF in this area, which mainly show a NE 60° orientation, it is reasonable to judge that the electrical orientation of this area is NE 60° on the whole. The rose-petal diagram of the electrical orientation of the sub-band shows similar characteristics to the full-band, which indicates that the electrical orientation of the study area is relatively uniform from shallow to deep and the linear characteristics are more evident.

3.4 Dimensional Analysis

The phase tensor invariant, φ_2, of each MT site was obtained using the phase tensor decomposition technique (Caldwell et al., 2004). The distribution characteristics of φ_2 with frequency can indicate the variation pattern of the apparent resistivity value below that MT site, which is actually the variation relationship of the apparent resistivity value with depth due to the correspondence between frequency and depth. When φ_2 is less than 45°, the apparent resistivity value below this MT site increases with depth, and when φ_2 is greater than 45°, the apparent resistivity value below this MT site decreases with depth (Heise et al., 2008). **Figure 2B** shows the distribution of the phase invariance, φ_2, with frequency for 34 sites along the profile. The electrical variation trends of the plots along the profile are not consistent, the electrical variation trends of the Ordos and Alxa Blocks are relatively simple, and the variation of φ_2 is mainly from high to low and then to high values, which shows that the stratigraphic characteristics of these two blocks are more clear. The value of φ_2 fluctuates more on both sides of the LPF and the high frequency part of the Langshan Mountain is dominated by a low phase, while the middle and low frequency parts are dominated by high frequency, and the φ_2 is larger than 70°. This shows that there may be an evident low-resistivity structure below the Langshan Mountain. In the Linhe Basin east of the LPF, the middle-high frequency part of φ_2 is dominated by high values (black dashed part in the figure), which indicates that there may be an existing, large-scale, low resistivity structure in the shallow part of the area, which corresponds to the existence of a thick, low-resistivity sedimentary layer in the Linhe Basin (Liang et al., 2021). The φ_2 in the low-frequency part of the Linhe Basin is dominated by low values, indicating that the resistivity values in the Linhe Basin show a significant increasing trend with increasing depth.

The phase tensor decomposition technique can also obtain the two-dimensional (2D) skewness angle ($|\beta|$) with a frequency distribution for each MT site. Considering the interference in the tectonic zone of LLA, it was determined that the subsurface medium could be approximated as a one-dimensional (1D) or 2D case when $|\beta|$ is less than 6, and the subsurface medium can be considered as a 3D case when $|\beta|$ is greater than 6. The larger the value of $|\beta|$, the stronger the three-dimensionality of MT data (Caldwell et al., 2004; Bibby et al., 2005; Cai et al., 2017). The high-frequency part of $|\beta|$ in the Linhe Basin is smaller (black dashed part in the figure), close to 0, and extends all the way to the vicinity of the Ordos Block, indicating that the shallow part of the region is an

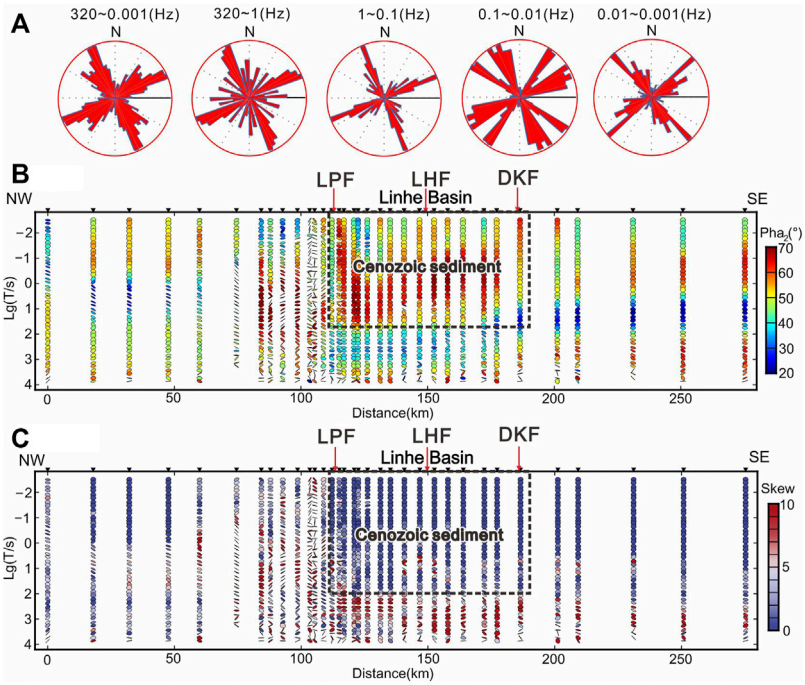

FIGURE 2 | Rose-petal diagram of the electrical orientation **(A)**, phase tensor invariant, φ_2 **(B)**, and two-dimensional skewness angle, |β| **(C)** of different periods of the profile.

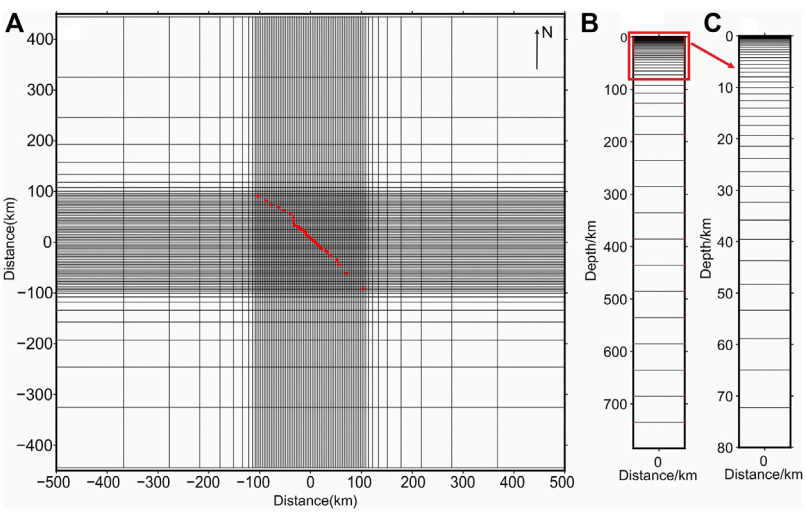

FIGURE 3 | Initial model used for the three-dimensional inversion of the study region **(A)** horizontal grid, **(B)** vertical grid, and **(C)** vertical grid of the target area. The red dots denote magnetotelluric (MT) sites.

approximately 1D or 2D laminar structure, which is presumed to be due to the thicker isotropic Cenozoic sedimentary layers, which is more similar to the distribution characteristics of φ_2 (**Figure 2C**). The overall |β| indicates that the Langshan Mountain is more complex than the Linhe Basin, while the smaller values of |β| in the Ordos and Alxa Blocks indicate that the tectonics of these two regions are relatively simple.

4 3D Inversion

In this study, the resistivity result model of the study area was calculated using the 3D inversion algorithm to invert the original data collected in the field. The latest version of the ModEM program (Egbert et al., 2012; Kelbert et al., 2014) was used and the full impedance tensor (four components: Zxx, Zxy, Zyx, and Zyy) was used as the input data for the 3D inversion calculation. A total

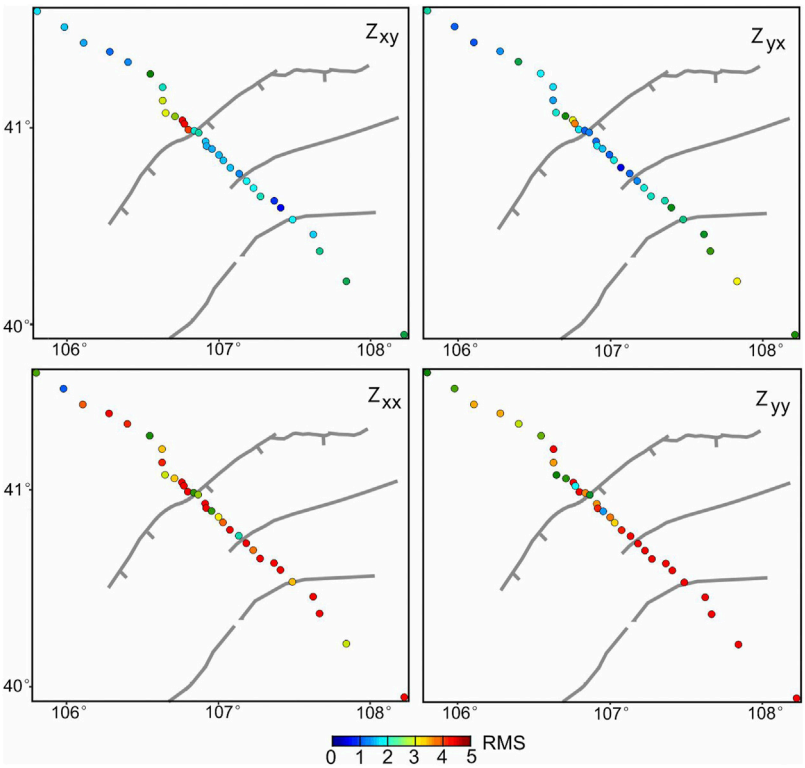

FIGURE 4 | Root mean square error (RMS) distribution of four components (Zxy, Zyx, Zxx, Zyy) at each magnetotelluric (MT) site of the three-dimensional inversion.

of 35 frequency points were used in the 3D inversion calculated from high to low frequency (**Supplementary Figure S5**). Before inversion calculation, data preparation and unified interpolation were carried out using MTP software (Chen et al., 2004) and Topeak software (Liu et al., 2017). The initial model grid was constructed using 3D inversion and was divided into horizontal and vertical grids (**Figure 3**). The horizontal grid was divided into the core part of the MT sites involved in the calculation and the expanded boundary grid. The horizontal grid of the core part was uniformly dissected using 3.0 × 3.0 km spacing, and a total of 60 (NS) × 60 (EW) grids were obtained. The extended boundary grid was constructed outside the core part by expanding 10 grids in four directions with 1.5 time multipliers. Finally, a total of 80 × 80 grids were constructed in the horizontal direction. The vertical grid design was similar to that of Cai (2017), Sun (2020) and Zhao (2022), and a total of 75 layers were obtained in the vertical direction.

In the 3D inversion calculation, the selection of data threshold error was consistent with the previous work of Sun (2020) and Zhao (2022). Since the diagonal components (Zxx, Zyy) were too small and the error was too large, we enlarged the error of the diagonal components in the actual 3D inversion and decreased the inversion weighting. The data threshold errors of diagonal components (Zxx, Zyy) and off-diagonal components (Zxy, Zyx) were set to 10% and 5%, respectively. A 100 Ω m uniform half space was used as the initial model and an automatically updated regularization factor was adopted. The initial value of the regularization factor was 5,000. When the inversion was no longer convergent, the regularization factor was updated to one 10th of the original value and the inversion was continued. The inversion was calculated many times and all data were carefully selected. After 65 iterations to the end of the inversion, the root mean square error (RMS) was reduced from 32 to 3.1. The RMS distribution map of each component for all 34 MT sites is shown in **Figure 4** and the detailed inversion process is shown in **Supplementary Figures S5–S7**; **Table S1**.

5 ELECTRICAL STRUCTURE IN THE LANGSHAN MOUNTAIN-LINHE BASIN AREA

Figure 5 shows the 3D inversion result within the depth range of 0–60 km along the profile. The topographical changes along the profile and the distribution of blocks and faults are drawn above the electrical structure image. The study area was divided into the Alxa Block, Langshan Mountain, Linhe Basin, and Ordos Block (Dong et al., 2016; Dong et al., 2018a, 2018b; He et al., 2020; Liang et al., 2021). Among them, the terrain of the Langshan Mountain fluctuates greatly, with an altitude of 1,500–2,300 m. The terrain of the Linhe Basin is relatively flat, and the average altitude is ~1,000 m (**Supplementary Figure S2**). The maximum altitude difference between the two blocks is up to thousands of meters, which is the location of LPF at the boundary of the two blocks. To

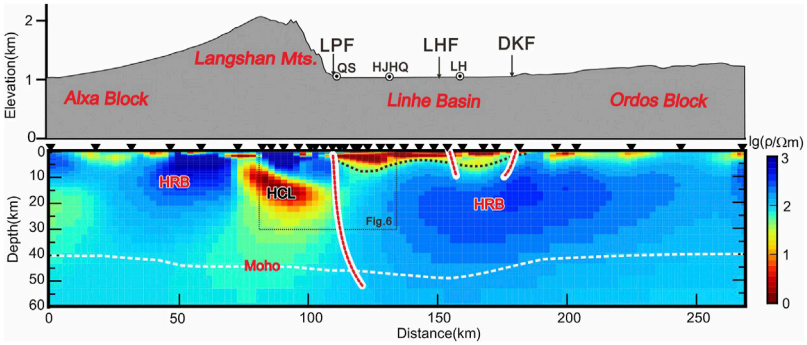

FIGURE 5 | Deep electrical structure map obtained using three-dimensional inversion and the topographical distribution map of the profile. The red dotted lines are the deep distribution of the fault inferred from the magnetotelluric (MT) results, and the black dotted line is the bottom boundary of the Cenozoic sedimentary layer inferred from the MT results. The white dotted line is distributed along the Moho surface (Chen et al., 2020).

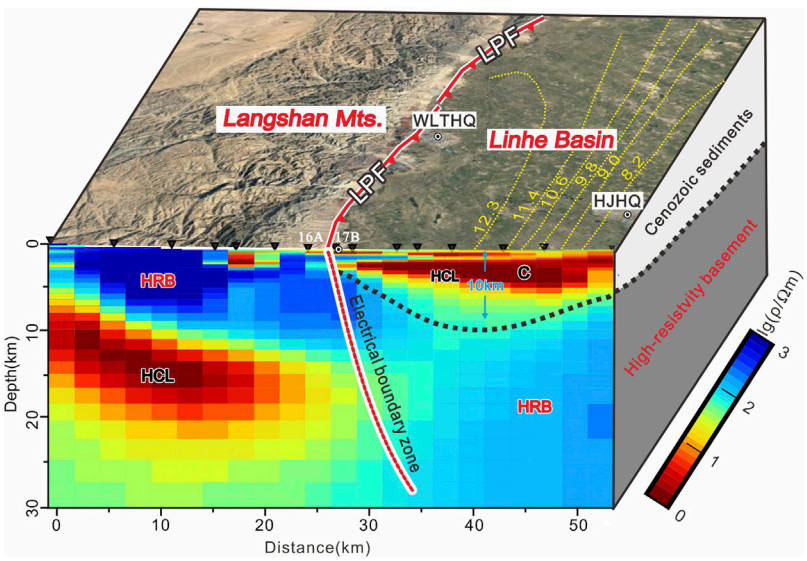

FIGURE 6 | Electrical structure and interpretation map of the core area of the Langshan Mountain-Linhe Basin area (the location is shown in the black dotted box in **Figure 1B**). The thickness of the Cenozoic sedimentary layer is quoted from the State Seismological Bureau (1988).

show the fine structure of LPF more intuitively and the sedimentary layer thickness of the Linhe Basin, the electrical structure and geomorphic distribution map within 30 km of the core area of LLA are drawn in **Figure 6** (the range is shown in the blue dotted box in **Figure 1** and **Figure 5**).

The LPF is an obvious electrical boundary zone between the Langshan Mountain and Linhe Basin, whether it is 10 km above or below the area (**Figure 5**). It is not only the boundary fault between the Langshan Mountain area and Linhe Basin, but also the largest main boundary fault in the study area. This corresponds to the view of Wen et al. (2014) that the structural deformation in the LLA is mainly distributed on the LPF. Dong et al. (2018a) revealed that the maximum sliding rate and maximum displacement of the fault are located in the middle of the fault, which is also where the MT profile passes through at this time. The upper crust in the Langshan Mountain area west of the LPF is a horizontally layered, high-resistivity body, with a depth of nearly 10 km as a whole, showing relatively complete high-resistivity characteristics, corresponding to the Paleozoic bedrock strata exposed in the Langshan Mountain area above (Rao et al., 2016; Dong et al., 2018a; 2018b; Zhang et al., 2020; Liang et al., 2021). The middle and lower crust of the Langshan Mountain area is dominated by a low-resistivity/high-conductivity layer (HCL), and there is a clear high and low electrical boundary zone between the middle and lower crust, and the high resistivity body structure of the upper crust at the bottom to 10 km, which indicates that the deep medium characteristics of the Langshan Mountain have a predominantly layered distribution. The HCL in **Figures 5**, **6** is a large-scale, low resistivity structure in the middle and lower

crust below the Langshan Mountain. Based on other geophysical data, such as the results of multi-scale tomography, we speculate that this may be due to the upwelling of mantle thermal materials and the transformation of the lithospheric structure of Langshan Mountain (Gao et al., 2018). There is a low-resistivity layer in the shallow part of the Linhe Basin to the east of LPF. The distribution of the low-resistivity layer is relatively flat on the profile, and the bottom depth is more than 5 km, becoming shallower and shallower to the east and extending near DKF.

To determine the specific location of LPF more accurately, intensive observation was carried out in the contact area between the Langshan Mountain and the Linhe Basin (**Figure 6**). It was determined that the accurate location of LPF is between the 2 MT sites, LSL1-16A and LSL1-17B (see **Supplementary Figure S4** for the apparent resistivity phase curve of all MT sites and the red triangle in **Figure 6**). The shallow part of the Linhe Basin is dominated by a low-resistivity layer, combined with 2D deviation angle |β| distribution (**Figure 6**). Previous geological survey results (Dong et al., 2016; He et al., 2017; 2018; 2020) speculate that these low-resistivity layers represent the Cenozoic sediments in the area, with evident 1D or 2D characteristics. The thickness of the low resistivity sedimentary layer near HJHQ in the hinterland of the Linhe Basin exceeds 10 km, which confirms the early geological survey that the Linhe Basin is a sedimentary basin with the largest thickness of sediment around the Ordos Block and that the Cenozoic sedimentary layer may reach 5–6 km (State Seismological Bureau, 1988). The latest research of Liang et al. (2021) found that the sedimentary layer of the Linhe Basin may be close to 10 km in the area crossed by the MT profile, which is similar to our results. Wu et al. (2022) recently obtained the large-scale, three-dimensional (3D) S-wave velocity structure of the crust and upper mantle of the Ordos Block and its surrounding areas, and found that there is a huge thickness of Cenozoic sedimentary layer in the Linhe Basin. The extremely thick Cenozoic sedimentary layer further reflects that the LLA has experienced continuous and strong tension, and normal fault depression sedimentary activities since the Cenozoic stage (State Seismological Bureau, 1988; Dong et al., 2018a; 2018b). It is one of the areas with the strongest tension in the Ordos Block. There is an evident high-resistivity body under the low-resistivity sedimentary layer in Linhe Basin. The high-resistivity basement is connected with the Ordos Block and extends to the hinterland of the Ordos Block, indicating that Linhe Basin and Ordos Block may belong to the same structural unit. The Alxa Block to the west of Langshan Mountain has high-resistivity and is a relatively simple structure. Ordos Block was also shown to be a relatively complete block unit, which is similar to the previous MT exploration results (Zhao et al., 2010; Dong et al., 2014; Li et al., 2017; Xu et al., 2017; Han et al., 2022). Through the two north-south MT profiles (Xu et al., 2017; Li et al., 2017) in Hetao Basin, it was found that the scale of the crust in the north of the Ordos Block is mainly a layered high resistivity body, which corresponds to our MT results. There is a low resistivity layer near the mantle. Our MT results this time did not find a similar situation, which may be due to the short profile. Our results reveal that the electrical structural characteristics of the Ordos Block are

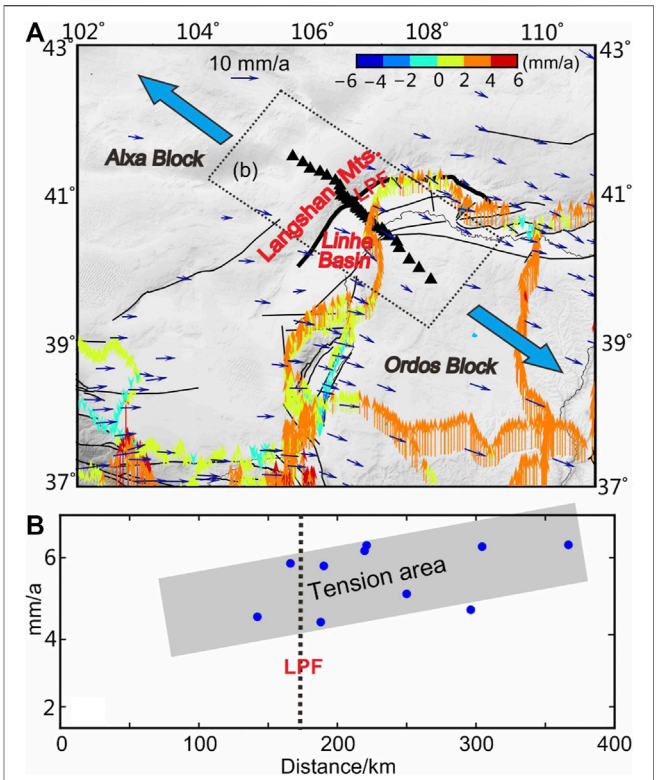

FIGURE 7 | Distribution map of the global positioning system (GPS) velocity field and leveling field in the study area and adjacent areas **(A)**, and GPS velocity decomposition **(B)** profile (blue arrow indicates the direction of regional stress field (modified from Zhang et al., 2006; Cui et al., 2016).

similar to those of Han et al. (2022) in the Helanshan Mountain-Yinchuan Basin. In addition, the electrical structural image in **Figure 5** shows that LHF and DKF in Linhe Basin are small in scale and do not pass through the high-resistivity body below the Linhe Basin and Ordos Block. These two faults belong to the internal faults of the Ordos Block. It is speculated that it may be an associated fault in the scale of upper crust formed during the process of tension in the structural area of LLA.

6 DYNAMIC ENLIGHTENMENT OF THE LANGSHAN MOUNTAIN-LINHE BASIN AREA

Active normal faults in China mainly develop around the Ordos Block (State Seismological Bureau, 1988). Except that the southwest edge of the Ordos Block is strike slip thrust, the rest are normal fault basins. Hetao Basin, including Linhe basin, is a sinistral shear tension zone (Fan et al., 2003; Chen et al., 2011). Since the Miocene, the Ordos Block has been characterized by NW–SE tensile stress and NE–SW compressive stress (Northrup et al., 1995; Zhang et al., 2006; Cui et al., 2016). Under the current tectonic stress field environment, the normal fault activity of the NE-distributed LPF coordinates the maximum normal strain produced by the regional stress field. In the active fault zone

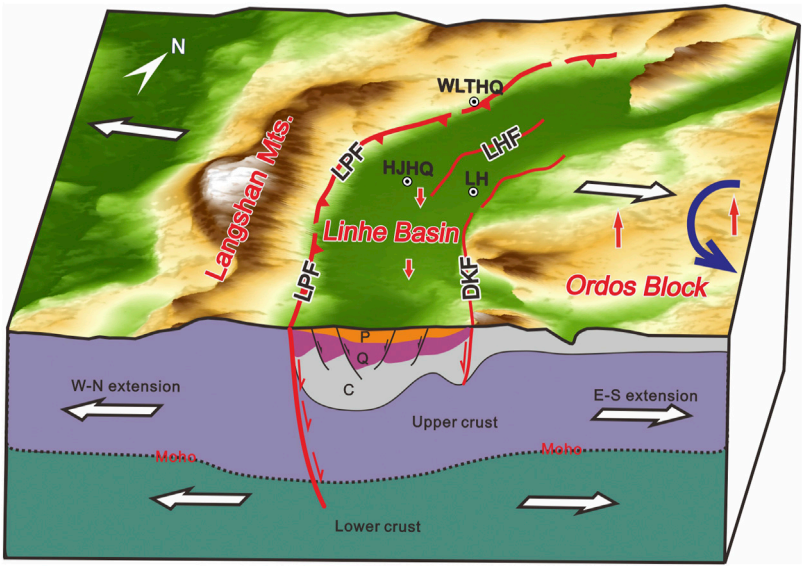

FIGURE 8 | Graphic of the tectonic movement mode in the Langshan Mountain-Linhe Basin area on the northwestern edge of the Ordos Block. The blue arrow represents the counterclockwise rotation of the Ordos Block; Moho quoted from Chen et al. (2020). P, Pleistocene; Q, Quaternary; C, Cenozoic (State Seismological Bureau, 1988)

around Ordos, the LPF may have a large seismic risk (Dong et al., 2018a, 2018b; Liang et al., 2021). The LPF has been located in the transition area between the Pacific extensional tectonic domain and the Tethys compression tectonic domain since the late Mesozoic (Ren et al., 2002; Zhang et al., 2006). It is a pre-existing, large-scale fault system. The study of the activity characteristics and trends of the fault is of great significance to earthquake prevention and disaster reduction in the Linhe Basin and even Hetao Basin (Rao et al., 2016; Dong et al., 2018a, 2018b; Zhang et al., 2020; Liang et al., 2021). Therefore, in addition to using the MT method to obtain the crustal scale electrical structural characteristics of LLA where the LPF is located, this study also used the GPS plane motion data of the study area from 2009 to 2015 (Hao et al., 2019) and the precise leveling vertical motion data from 1970 to 2014 (Hao et al., 2016) recently obtained by the second monitoring center of the China Earthquake Administration. The combination of static deep electrical structure data and dynamic 3D crustal movement field data provides better constraints for the establishment of geodynamic models in the Linhe Basin and the periphery of the Ordos Block, and provides reliable reference data for seismic risk assessment in the LLA area.

Figure 7A shows the GPS velocity distribution field of LLA and its adjacent areas relative to the Eurasian block from 2009 to 2015 (blue plane arrow) and the annual vertical deformation field of LLA and its adjacent areas relative to the Ordos Block obtained from precise leveling data from 1970 to 2014 (color vertical arrow) (data quoted from Hao et al., 2016; 2019). The GPS velocity field within the black box is decomposed into the direction along the MT profile (**Figure 7B**; the north and east are positive). The GPS velocity field shows an overall trend of SE movement in the study area, and the GPS velocity field values show an increasing trend from the Alxa Block through the LLA to the Ordos Block, increasing from 4 mm/a to 7 mm/a. This shows that the LLA is an evident accelerating zone, indicating that the area is undergoing continuous NW–SE tension. Current research on tectonic stress fields shows that the fault depression system around the Ordos Block, including the structural area of LLA, shows NW–SE horizontal tensile stress (Zhang et al., 2006; Cui et al., 2016), which corresponds to the results obtained in this study. The precise leveling data from 1970 to 2014 indicate that the Linhe Basin is dominated by uplift (colored vertical arrow in **Figure 7A**), and the uplift rate is approximately 0–2 mm/a, which is less than the annual uplift rate of 2–4 mm/a in the hinterland of the Ordos Block (Hao et al., 2016). The Linhe Basin and Ordos Block belong to the same tectonic unit, while the Linhe Basin shows subsidence relative to the Ordos Block, which may be due to the strong tension in LLA. A movement model map of LLA on the northwest edge of the Ordos Block is postulated (**Figure 8**). As the Ordos and Alxa Blocks are currently subjected to the NE pushing of the Tibetan Plateau and the deep subduction and extension of the Pacific plate (Northrup et al., 1995; Zhang et al., 2006), the two blocks continue to carry out evident separation activities, resulting in normal tension fault depression sedimentary activities in LLA, forming a huge fault depression basin. The LPF is the boundary fault between the two blocks and there is concomitantly a strong risk of earthquake preparation.

7 CONCLUSION

Broadband magnetotelluric exploration was carried out across the LLA in the NW–SE direction, and the 3D, deep electrical structure revealed that the LPF in the LLA was an evident

electrical boundary zone on the whole crustal scale and is the main boundary fault of the primary structural block of the Alxa and Ordos Blocks. The MT results also show that Linhe Basin and Ordos Block belong to the same tectonic basement. The Linhe fault (LHF), and Dengkou fault (DKF) belong to the internal faults of the Ordos Block. The upper crust of the Langshan Mountain on the west side of LPF is characterized by high-resistivity, the middle and lower crust have low-resistivity, and the Linhe basin on the east side has a Cenozoic, low-resistivity sedimentary layer of ~5–10 km thick. This indicates that the Linhe Basin is a faulted basin with sedimentary thickness near the Ordos Block, reflecting that the LLA has experienced continuous and strong tension and normal fault depression sedimentary activities since the Cenozoic stage. The current GPS velocity field shows that there is an evident NW–SE accelerating zone in the LLA. The leveling data indicate that the Linhe Basin shows a subsidence trend relative to the Ordos Block, indicating that the area is undergoing continuous NW–SE tension and faulting. It is speculated that there is a risk of earthquake preparation in the LPF.

DATA AVAILABILITY STATEMENT

The raw data supporting the conclusion of this article will be made available by the authors, without undue reservation.

AUTHOR CONTRIBUTIONS

LZ completed the field data acquisition, the data analyses, and wrote the article. QW provided funding for the study. CC assisted in data acquisition. MH provided GPS and leveling data. All authors contributed to manuscript revision and discussion and approved the submitted version.

FUNDING

This paper is jointly funded by the National Key Research and Development Plan (2017YFC1500100), the Open Fund of the State Key Laboratory of Seismic Dynamics (LED 2019B06, LED 2021B04), and the National Field Scientific Observation and Research Station Project of Continental Rift Dynamics in Taiyuan, Shanxi Province (NORSTY 20-07).

ACKNOWLEDGMENTS

Sun Shufeng, Li Xi'an, Li Fengquan and others provided help in the process of field data acquisition. Researcher Chen Xiaobin of the National Institute of Natural Hazards, Ministry of Emergency Management of China and Dr. Liu Zhongyin of the Institute of Geology, China Earthquake Administration provided MTP and Topeak series software for the 3D inversion calculation and gave detailed guidance; Dr. Xu Jianhong of the Second Monitoring and Application Center, China Earthquake Administration, provided help in structural interpretation.

SUPPLEMENTARY MATERIAL

The Supplementary Material for this article can be found online at: https://www.frontiersin.org/articles/10.3389/feart.2022.916044/full#supplementary-material.

REFERENCES

Bibby, H. M., Caldwell, T. G., and Brown, C. (2005). Determinable and Non-determinable Parameters of Galvanic Distortion in Magnetotellurics. *Geophys. J. Int.* 163, 915–930. doi:10.1111/j.1365-246X.2005.02779.x

Cai, J., Chen, X., Xu, X., Tang, J., Wang, L., Guo, C., et al. (2017). Rupture Mechanism and Seismotectonics of the M S 6.5 Ludian Earthquake Inferred from Three-dimensional Magnetotelluric Imaging. *Geophys. Res. Lett.* 44, 1275–1285. doi:10.1002/2016GL071855

Caldwell, T. G., Bibby, H. M., and Brown, C. (2004). The Magnetotelluric Phase Tensor. *Geophys. J. Int.* 158, 457–469. doi:10.1111/j.1365-246X.2004.02281.x

Chang, C., Wang, H., Gao, R., Guo, H., Han, S., and Wu, Y. (2022). Deep Crustal Structure of the Eastern Central Asian Orogenic Belt Revealed by Integrated Magnetic-Gravity Imaging. *Front. Earth Sci.* 10, 843499. doi:10.3389/feart.2022.843499

Chang, L., Wang, C., and Ding, Z. (2011). Study on the Anisotropy of Ordos Block and Surrounding Upper Mantle. Study on the Anisotropy of Ordos Block and Surrounding Upper Mantle. *Sci. China Earth Sci.* 41, 686–699. doi:10.1360/zd-2011-41-5-686

Chen, L., and Wang, G. (1990). *Magnetotelluric Sounding method[M]*. Beijing:: Geological Publishing House, 10–15.

Chen, X., Zhao, G., and Zhan, Y. (2004). A Visual Intergrated Windows System for MT Data Process and Interpretation. *Oil Geophys.Pro* 39 (Suppl. l.), 11–16. CNKI:SUN:SYDQ.0.2004-S1-004.

Chen, Y., Chen, J., Guo, B., Li, S., Qi, S., Zhao, P., et al. (2020). Crustal Structure and Deformation between Different Blocks in the Northern Part of the Western Margin of Ordos. *Chin. J. Geophys.* 63, 886–896. doi:10.6038/cjg2020N0211

Cui, D., Hao, M., Li, Y., Wang, W., Qin, S., and Li, Z. (2016). Present-day Crustal Movement and Strain of the Surrounding Area of Ordos Block Derived from Repeated GPS Observations. *Chin. J. Geophys (in Chin.* 59 (10), 3646–3661. doi:10.6038/cjg20161012

Deng, Q., Zhang, P., Ran, Y., Yang, X., Min, W., and Chen, L. (2003). Active Tectonics and Earthquake Activities in China. *Earth Sci. Front.* 10 (Suppl. l), 66–73.

Dong, H., Wei, W., Ye, G., Jin, S., Jones, A. G., Jing, J., et al. (2014). Three-dimensional Electrical Structure of the Crust and Upper Mantle in Ordos Block and Adjacent Area: Evidence of Regional Lithospheric Modification. *Geochem. Geophys. Geosyst.* 15, 2414–2425. doi:10.1002/2014GC005270

Dong, S. (2016). *Study on Late Quaternary Activity Habits and Paleoearthquakes of Langshan Piedmont Fault*. China Earthquake Adaministration. Beijing, China: Institute of Geology. Doctoral thesis.

Dong, S., Zhang, P., Zhang, H., Zheng, W., and Chen, H. (2018a). Drainage Responses to the Activity of the Langshan Range-Front Fault and Tectonic Implications-Front Fault and Tectonic Implications. *J. Earth Sci.* 29 (1), 193–209. doi:10.1007/s12583-017-0902-8

Dong, S., Zhang, P., Zheng, W., Lei, Q., Yang, H., Liu, J., et al. (2018b). Paleoseismic Study of Langshan Piedmont Fault in Hetao Area. *Seismol. Geo* 40 (6), 1216–1239. doi:10.3969/j.issn.0253-4967.2018.06.003

Dong, S., Zhang, P., Zheng, W., Yu, Z., Lei, Q., Yang, H., et al. (2018c). Paleoseismic Observations along the Langshan Range-Front Fault, Hetao Basin, China: Tectonic and Seismic Implications. *Tectonophysics* 730, 63–80. doi:10.1016/j.tecto.2018.02.012

Du, J., Li, D., Wang, Y., and Ma, Y. (2017). Late Quaternary Activity of the Huashan Piedmont Fault and Associated Hazards in the Southeastern Weihe Graben, Central China. *Acta Geol. Sin. - Engl. Ed.* 91 (1), 76–92. doi:10.1111/1755-6724.13064

Egbert, G. D., and Kelbert, A. (2012). Computational Recipes for Electromagnetic Inverse Problems. *Geophys.J. Int.* 189, 251–267. doi:10.1111/j.1365-246X.2011.05347.x

Fan, J., Ma, J., and Gan, W. (2003). Movement of Ordos Block and Alternation of Activity along its Boundaries. *Sci. China Earth* 46 (Suppl. p), 168–180. doi:10.1360/03dz0013

Feng, X., Ma, J., Zhou, Y., England, P., Parsons, B., Rizza, M. A., et al. (2020). Geomorphology and Paleoseismology of the Wein-An Fault, Shaanxi, Central China, and the Source of the 1556 Huaxian Earthquake. *J. Geophys. Res. Solid Earth* 125, e2019JB017848. doi:10.1029/2019jb017848

Gao, X., Guo, B., Chen, J., Liu, Q., Li, S., and Li, Y. (2018). Rebuilding of the Lithosphere beneath the Western Margin of Ordos: Evidence from Multiscale Seismic Tomography. *Chin. J. Geophys* 61 (7), 2736–2749. doi:10.6038/cjg2018L0319

Han, J., Zhao, L., Sun, X., Zhan, Y., and Liu, X. (2022). Electrical Structures of the Yinchuan Basin and Adjacent Area, Western North China Craton, Inferred from Magnetotelluric Imaging. *J. of Asian Earth Sci.* 227, 105089. doi:10.1016/j.jseaes.2022.105089

Hao, M., Li, Y., and Zhuang, W. (2019). Crustal Movement and Strain Distribution in East Asia Revealed by GPS Observations. *Sci. Rep.* 9, 16797. doi:10.1038/s41598-019-53306-y

Hao, M., Wang, Q., Cui, D., Liu, L., and Zhou, L. (2016). Present-day Crustal Vertical Motion Around the Ordos Block Constrained by Precise Leveling and GPS Data. *Surv. Geophys* 37 (5), 923–936. doi:10.1007/s10712-016-9375-1

He, Z., Ma, B., Hao, Y., Zhao, J., and Wang, J. (2020). Surface Rupture Geomorphology and Vertical Slip Rates Constrained by Terraces along the Wulashan Piedmont Fault in the Hetao Basin, China. *Geomorphology* 358, 107–116. doi:10.1016/j.geomorph.2020.107116

He, Z., Ma, B., Long, J., Wang, J., and Zhang, H. (2018). New Progress in Paleoearthquake Studies of the East Sertengshan Piedmont Fault, Inner Mongolia, China. *J. Earth Sci.* 29 (2), 441–451. doi:10.1007/s12583-017-0937-z

He, Z., Ma, B., Long, J., Zhang, H., Liang, K., and Jiang, D. (2017). Recent Ground Fissures in the Hetao Basin, Inner Mongolia, China. *Geomorphology* 295, 102–114. doi:10.1016/j.geomorph.2017.07.008

Heise, W., Caldwell, T. G., Bibby, H. M., and Bannister, S. C. (2008). Three-dimensional Modelling of Magnetotelluric Data from the Rotokawa Geothermal Field, Taupo Volcanic Zone, New Zealand. *Geophys. J. Int.* 173, 740–750. doi:10.1111/j.1365-246X.2008.03737.x

Hou, J.-J., Han, M.-K., Chai, B.-L., and Han, H.-Y. (1998). Geomorphological Observations of Active Faults in the Epicentral Region of the Huaxian Large Earthquake in 1556 in Shaanxi Province, China. *J. of Struct. Geol.* 20 (5), 549–557. doi:10.1016/S0191-8141(97)00112-0

Hu, X., Lin, W., Yang, W., and Yang, B. (2020). Research Progress on Electrical Structure of Cratonic Lithosphere. *Sci. China Earth* 50, 1533–1552. doi:10.1360/SSTe-2019-0141

Hu, Y., Cui, D., Ji, L., and Hao, M. (2011). Seismic Anisotropy of Upper Mantle in Ordos Block and Adjacent Regions. *Chin. J. Geophys* 54 (6), 1549–1558. doi:10.3969/j.issn.0001-5733.2011.06.014

Jia, L., Zhang, X., Ye, P., Zhao, X., He, Z., He, X., et al. (2016). Development of the Alluvial and Lacustrine Terraces on the Northern Margin of the Hetao Basin, Inner Mongolia, China: Implications for the Evolution of the Yellow River in the Hetao Area since the Late Pleistocene. *Geomorphology* 263, 87–98. doi:10.1016/j.geomorph.2016.03.034

Kelbert, A., Meqbel, N., Egbert, G. D., and Tandon, K. (2014). ModEM: A Modular System for Inversion of Electromagnetic Geophysical Data. *Comput. Geosciences* 66, 40–53. doi:10.1016/j.cageo.2014.01.010

Lei, Q., Chai, C., Du, P., Yu, J., Wang, Y., and Xie, X. (2015). The Seismogenic Structure of the M8.0 Pingluo Earthquake in 1739. *Seismol. Geo.* 37, 413–429. doi:10.3969/j.issn.0253-4967.2015.02.006

Li, C., Bai, D., Xue, S., Li, X., Ma, X., Yan, Y., et al. (2017). A Magnetotelluric Study of the Deep Electric Structure beneath the Ordos Block. *Chin. J. Geophys* 60 (5), 1788–1799. doi:10.6038/cjg20170515

Li, J., Ye, T., Zhang, H., and Huang, Q. (2021a). A Multi-Geophysical Parameter Model in Tengchong Volcanic Area. *Chin. J. Geophys* 64 (10), 3657–3668. doi:10.6038/cjg2021P0214

Li, L., Li, D., Lv, Y., and Shi, J. (2021b). The Late Quaternary Mountain-Front Terrace Sequences along the Langshan Mountains: Implications for the Evolution of the Western Hetao Graben. *Nat. Haz. Res.* 1 (3), 109–115. doi:10.1016/j.nhres.2021.07.001

Li, Y., Ran, Y., Chen, L. C., Wu, F., and Lei, S. X. (2015). The Latest Surface Rupture Events on the Major Active Faults and Great Historical Earthquakes in Hetao Fault-Depression Zone. *Seismol. Geo* 37 (1), 110–125. doi:10.3969/j.issn.0253-4967.2015.01.009

Liang, K., He, Z., Ma, B., Tian, Q., and Liu, S. (2021). Joint-rupture Pattern and Newly Generated Structure of Fault Intersections on the Northern Margin of the Linhe Basin, Northwestern Ordos Block, China. *Tectonics* 40, e2021TC006845. doi:10.1029/2021tc006845

Liu, Z., Chen, X., and Cai, J. (2017). toPeak: A Visual Client Software for Magnetotelluric Three-Dimensional Inversion. 13th China International Geophysical Symposium, Wuhan, China.

Northrup, C. J., Royden, L. H., and Burchfiel, B. C. (1995). Motion of the Pacific Plate Relative to Eurasia and its Potential Relation to Cenozoic Extension along the Eastern Margin of Eurasia. *Geol* 23, 719–722. doi:10.1130/0091-7613(1995)023<0719:motppr>2.3.co;2

Rao, G., Chen, P., Hu, J., Yu, Y., and Qiu, J. (2016). Timing of Holocene Paleo-Earthquakes along the Langshan Piedmont Fault in the Western Hetao Graben, North China: Implications for Seismic Risk. *Tectonophysics* 677-678, 115–124. doi:10.1016/j.tecto.2016.03.035

Rao, G., Lin, A., Yan, B., Jia, D., and Wu, X. (2014). Tectonic Activity and Structural Features of Active Intracontinental Normal Faults in the Weihe Graben, Central China. *Tectonophysics* 636, 270–285. doi:10.1016/j.tecto.2014.08.019

Ren, J., Tamaki, K., Li, S., and Zhang, J. (2002). Late Mesozoic and Cenozoic Rifting and its Dynamic Setting in Eastern China and Adjacent Areas. *Tectonophysics* 344 (3), 175–205. doi:10.1016/S0040-1951(01)00271-2

Siripunvaraporn, W., Egbert, G., Lenbury, Y., and Uyeshima, M. (2005). Three-dimensional Magnetotelluric Inversion: Data-Space Method. *Phys. of Earth Planet. Interiors* 150, 3–14. doi:10.1016/j.pepi.2004.08.023

State Seismological Bureau (1988). *Active Fault System Around Ordos Massif*. Beijing, China: Seismological Press.

Sun, X., Zhan, Y., Unsworth, M., Egbert, G., Zhang, H., Chen, X., et al. (2020). 3-D Magnetotelluric Imaging of the Easternmost Kunlun Fault: Insights into Strain Partitioning and the Seismotectonics of the Jiuzhaigou Ms7.0 Earthquake. *J. Geophys. Res. Solid Earth.* 125, e2020JB019731. doi:10.1029/2020jb019731

Sun, X., Zhan, Y., Zhao, L., Chen, X., Sun, J., Li, C., et al. (2019). Electrical Structure of the Kunlun-Qinling Fault System, Northeastern Tibetan Plateau, Inferred from 3-D Inversion of Magnetotelluric Data. *J. of Asian Earth Sci.* 181, 103910. doi:10.1016/j.jseaes.2019.103910

Wang, X., Zhang, G., Zhou, J., Li, D., Luo, W., Hu, Y., et al. (2018). Crust and Upper Mantle Electrical Resistivity Structure in the Longmenshan Tectonic Belt and its Relationship with Wenchuan and Lushan Earthquakes. *Chin. J. Geophys* 61 (5), 1984–1995. doi:10.6038/cjg2018M0233

Wen, X. (2014). Structure of Source Regions of the 1979 Ms 6.0 Wuyuan Earthquake and the 1996 Ms 6.4 Baotou Earthquake in Inner Mongolia, China. *Seismol. Geo* 36 (3), 586–597. doi:10.3969/j.issn.0253-4967.2014.03.004

Wu, J., Liu, Y., Zhong, S., Wang, f., Cai, Y., Wang, W., et al. (2022). Joint Inversion of Receiver Function and Surface Wave of Lithospheric Structure in Ordos Block and its Surrounding Areas. *Sci. China Earth*. pre publication. doi:10.1360/SSTe-2021-0275

Xu, D., He, Z., Ma, B., Long, J., Zhang, H., and Liang, K. (2022). Vertical Slip Rates of Normal Faults Constrained by Both Fault Walls: A Case Study of the Hetao Fault System in Northern China. *Front. Earth Sci.* 10, 816922. doi:10.3389/feart.2022.816922

Xu, L., Wei, W., Jin, S., Ye, G., Liang, H., Jia, C., et al. (2017). Study of Deep Electrical Structure along a Profile from Northern Ordos Block to Yinshan Orogenic Belt. *Chin. J. Geophys* 60 (2), 575–584. doi:10.6038/cjg20170212

Xu, Y., He, H., Deng, Q., Allen, M. B., Sun, H., and Bi, L. (2018). The CE 1303 Hongdong Earthquake and the Huoshan Piedmont Fault, Shanxi Graben: Implications for Magnitude Limits of Normal Fault Earthquakes. *J. Geophys. Res. Solid Earth* 123 (4), 3098–3121. doi:10.1002/2017JB014928

Ye, T., Chen, X., Huang, Q., and Cui, T. (2021). Three-dimensional Electrical Resistivity Structure in Focal Area of the 2021 Yangbi MS6.4 Earthquake and its Implication for the Seismogenic Mechanism. *Chin. J. Geophys* 64 (7), 2267–2277. doi:10.6038/cjg2021O0523

Yu, N., Hu, X., Li, J., Zhao, N., Zhou, J., Cai, X., et al. (2017). Electrical Structure of the Longling Area in Western Yunnan and its Effect on Route Selection of the Dali-Ruili Railway. *Chin. J. Geophys* 60 (6), 2442–2455. doi:10.6038/cjg20170632

Zhan, Y., Liang, M., Sun, X., Huang, F., Zhao, L., Gong, Y., et al. (2021). Deep Structure and Seismogenic Pattern of the 2021.5.22 Madoi(Qinghai) Ms 7.4 Earthquake. *Chin. J. Geophys* 64 (7), 2232–2252. doi:10.6038/cig2021O0521

Zhan, Y., Yang, H., Zhao, G., Zhao, L., and Sun, X. (2017). Deep Electrical Structure of Crust beneath the Madongshan Step Area at the Haiyuan Fault in the Northeastern Margin of the Tibetan Plateau and Tectonic Implications. *Chin. J. Geophys.* 60, 2371–2384. doi:10.6038/cig20170627

Zhang, J., Cunningham, D., Yun, L., Qu, J., Zhao, H., Zhang, B., et al. (2021). Kinematic Variability of Late Cenozoic Fault Systems and Contrasting Mountain Building Processes in the Alxa Block, Western china. *J. of Asian Earth Sci.* 205, 104597. doi:10.1016/j.jseaes.2020.104597

Zhang, R., Zhang, Z., Zheng, D., Liu, X., Lei, Q., and Shao, Y. (2021). Coulomb Stress Transfer of Strong Earthquakes within Tectonic Belts Near Western Ordos Block. *Chin. J. Geophys* 64 (10), 3576–3599. doi:10.6038/cjg2021P0008

Zhang, Y., Liao, C., Shi, W., and Bo, H. (2006). Neotectonic Evolution of the Peripheral Zones of the Ordos Basin and Geodynamic Setting. *Geol. J. of China Univ.* 12, 285–297.

Zhao, C., Zhang, L., Yu, P., and Xu, X. (2021). Integrated Geophysical Evidence for the Middle-Lower Crust Melting of the Songpan-Aba Terrain, NE Tibetan Plateau. *Front. Earth Sci.* 9, 752693. doi:10.3389/feart.2021.752693

Zhao, G., Tang, J., Zhan, Y., Chen, X., Zhuo, X., Wang, J., et al. (2004). Study on the Relationship between Crustal Electrical Structure and Block Deformation in the Northeast Margin of Qinghai Xizang Plateau, Sci. *China Earth Sci.* 34 (10), 908–918.

Zhao, G., Unsworth, M. J., Zhan, Y., Wang, L., Chen, X., Jones, A. G., et al. (2012). Crustal Structure and Rheology of the Longmenshan and Wenchuan Mw 7.9 Earthquake Epicentral Area from Magnetotelluric Data. *Geology* 40, 1139–1142. doi:10.1130/G33703.1

Zhao, G., Zhan, Y., Wang, L., Wang, J., Tang, J., Chen, X., et al. (2010). Crustal Electrical Structure of Ordos Fault Block. *Seismol. Geo* 32, 345–359.

Zhao, L., Zhan, Y., Wang, Q., Sun, X., Hao, M., Zhu, Y., et al. (2022). 3D Electrical Structure and Crustal Deformation of the Lajishan Tectonic Belt, Northeastern Margin of the Tibetan Plateau. *J. of Asian Earth Sci.* 224, 104953. ISSN 1367-9120. doi:10.1016/j.jseaes.2021.104953

Conflict of Interest: The authors declare that the research was conducted in the absence of any commercial or financial relationships that could be construed as a potential conflict of interest.